Low coverage spontaneous etching and hyperthermal desorption of aluminum chlorides from Cl_2/Al(111)

Tyler J. Grassman, Gary C. Poon, and Andrew C. Kummel
Department of Chemistry and Biochemistry, University of California, San Diego, 9500 Gilman Drive, Mail Code 0358, La Jolla, California 92093-0358

(Received 1 August 2003; accepted 18 August 2004)

Nonresonant multiphoton ionization with time-of-flight mass spectrometry has been used to monitor the desorption of aluminum chloride (Al_xCl_y) etch products from the Al(111) surface at 100 and 500 K during low-coverage (<5% monolayer) monoenergetic Cl_2 (0.11–0.65 eV) dosing. The desorption products in this low-coverage range show predominantly hyperthermal exit velocities under all dosing conditions. For example, with 0.27 eV incident Cl_2, the etch product was found to have a most-probable velocity of 517 ± 22 m/s at an Al(111) surface temperature of 100 K. This corresponds to 22 times the expected thermal desorption translational energy for $AlCl_3$. Cl_2 sticking probability measurements and Al_xCl_y etch rate measurements show etching even at Cl_2 coverages of less than 5% monolayer at surface temperatures between 100 and 500 K. These experimental results are consistent with a combination of fast-time-scale surface diffusion and agglomeration of the adsorbed chlorine to form aluminum chlorides and the presence of activated $AlCl_3$ chemisorption states having potential energies above the vacuum level. Density functional theory calculations yield results that are consistent with both our experimental findings and mechanistic descriptions. © *2004 American Institute of Physics.* [DOI: 10.1063/1.1805495]

I. INTRODUCTION

The mechanism of Cl_2 adsorption onto aluminum, and subsequent etching by thermal aluminum chloride desorption, has been studied many times in the last quarter century.[1–13] Most of the work has focused on Cl_2 plasma etching for integrated circuit processing of aluminum films. Because plasma etching environments are typically very complex, the problem is usually broken down into much simpler components, including the dry etching of Al by Cl_2. Etch rate and etch product studies utilizing a variety of techniques, including (but not limited to) quadrupole[1–3] and time-of-flight mass spectrometry,[5] gas-phase titration of chlorine atoms,[6] quartz-crystal microbalance,[2,4] *in situ* Fourier transform infrared spectroscopy,[7] Auger electron spectroscopy,[4,10–12] and x-ray photoelectron spectroscopy[1,4] have been performed at pressures ranging from ultrahigh vacuum (UHV) to near atmospheric. Kinetic modeling has also been employed to characterize the processes involved in both the thermal and ion-assisted etching of Al(111) by Cl_2.[9]

Spontaneous high-rate thermal etching of Al by Cl_2 has been reported by several investigators at high surface coverages (monolayer or greater).[1–10] These reports state that at least monolayer coverages of chlorine are necessary for the initiation of thermal desorption of aluminum chloride etch products. Presumably this high chlorine coverage allows for subsurface absorption of Cl adsorbates to occur such that the surface Al atoms are more stoichiometrically surrounded by Cl atoms.[11] These stoichiometric aluminum chlorides are then said to thermally desorb into the gas phase with a barrier to desorption equal to about room temperature. This thermal etching is reported to be quenched below room temperature;[6] ion-assisted etching has been observed at −50 °C in electron cyclotron resonance (ECR) plasmas.[9] These proposed high-coverage adsorption and etching mechanisms reproduce the experimental high-coverage data reasonably well.

Conversely, we observe not only that etching of Al(111) by Cl_2 can occur at very low surface coverages (<5% monolayer), but that these etch products actually exit the surface at hyperthermal velocities which correspond to 2–30 times thermal energy. Remarkably, these effects are independent of both surface temperature (experiments were done at both 100 and 500 K) and Cl_2 translational energy (0.11, 0.27, and 0.65 eV Cl_2 incident energies were studied). Time-of-flight mass spectrometry of aluminum chloride desorption products, Cl_2 sticking probability measurements, and etch rate profiling experiments (etch rate vs Cl_2 exposure time) all clearly indicate a low-coverage hyperthermal etching behavior that has not yet been reported. Computational density functional theory (DFT) modeling of the Cl_2/Al(111) gas-surface reaction sequence has also been performed to further characterize the mechanism behind this etching phenomenon. We have thus developed a mechanistic model to account for both the occurrence of the low-coverage etching and the hyperthermicity of the desorbed etch products. We hypothesize that the ultralow-coverage etch results from reactions of Cl adsorbates with exposed, and therefore more reactive, Al surface defect-type sites such as adatoms, regrowth islands, and step edges. It is at these special sites, then, that the subsequently formed aluminum chloride reaction product is able to exist in a slightly energized or excited state, specifically an activated chemisorption state, with a potential energy above that of the vacuum level. Thereafter, desorption produces

etch products that exit the surface with translational energies greater than that of thermal energy.

II. METHODS

A. Experimental setup

All experiments were performed under UHV conditions with a base chamber pressure of 2×10^{-10} Torr. The UHV chamber used for these studies has been previously described in detail elsewhere.[14–17,20] Experiments were performed on an aluminum single crystal (Monocrystals Company, 99.999+% purity, 10 mm diameter×2 mm thickness) with a (111) surface orientation. The aluminum surface was cleaned by sputtering with normal incidence 2 kV Ar^+ ions; this was followed by a two minute high temperature anneal (500 °C) to reduce sputter damage. Surface purity and order were then checked by Auger electron spectroscopy and low-energy electron diffraction.

Aluminum chloride desorption experiments were performed in conjunction with Cl_2/Al(111) abstractive chemisorption measurements.[18] A mechanically chopped (7 μs chopper open time), 10 Hz pulsed molecular beam (General Valve, model 9-400-900, 2 mm orifice) of Cl_2 seeded in different noble gases was used to dose the aluminum surface at three different Cl_2 incident energies: pure Cl_2 at 0.11 ± 0.01 eV, 5% Cl_2/Ne at 0.27 ± 0.01 eV, and 5.32% Cl_2/He at 0.65 ± 0.02 eV. (Note that all values reported in this paper, where applicable, are given with standard errors, rather than standard deviations, because the reported numbers are mean values of numerous experiments.) All related etching experiments were performed with the molecular beam at normal incidence to the surface, and products were detected just off-normal (~9° off of the surface perpendicular) in an effort to avoid interference from the incident beam.

All gases were purchased premixed from Matheson Tri-Gas, and no other halogen contaminants were detected by quadrupole mass spectrometer (QMS). The average beam fluxes—as calculated via half surface coverage times from sticking data, and using a simple $1-\theta$ sticking coefficient dependence—were found to be as follows: 3.0×10^{13} molecules cm^{-2} sec^{-1} for pure Cl_2, 2.6×10^{13} molecules cm^{-2} sec^{-1} for Cl_2/Ne, and 1.0×10^{13} molecules cm^{-2} sec^{-1} for Cl_2/He. All three molecular beam varieties gave an increase in background pressure of no more than 2×10^{-11} Torr when introduced into the main UHV chamber.

The aluminum chloride desorption products were detected via nonresonant multiphoton ionization (MPI) and subsequent time-of-flight mass spectrometry (TOF-MS). A pulsed UV laser was optimized for resonant multiphoton ionization of neutral chlorine atoms, but also provided sufficient fluence for both the dissociation of the aluminum chloride desorption products and a strong nonresonant aluminum MPI signal, as described by Eqs. (1) and (2):

$$Al_xCl_y \xrightarrow{nh\nu} xAl + yCl, \tag{1}$$

$$Al \xrightarrow{nh\nu} Al^+. \tag{2}$$

The laser light was prepared by using the frequency-doubled fundamental from a *Q*-switched Nd:YAG (YAG—yttrium aluminum garnet) laser (Continuum, 581C-SF; 532 nm, 10 Hz, 7 ns pulse width) to pump a tunable dye laser (Lambda-Physik, FL 3002) running DCM/methanol, tuned to 630.6 nm. The dye laser output was frequency-doubled with a KDP-C (KDP-C—potassium dihydrogen phosphate-carbon) crystal housed in a wavelength-tracking package (Inrad, UV Autotracker III). This doubled light was then added to the remaining dye laser fundamental (via a BBO crystal in an identical Autotracker box) to produce a final output of 210.2 nm, with average pulse energy of 1.5 mJ, pulse widths of 7 ns, and a rate of 10 Hz.

Experiments were performed at aluminum surface temperatures of both 100 and 500 K. The TOF detection method was used to probe incident and scattered species (Cl_2), as well as abstraction (Cl) and desorption (Al_xCl_y) products. Sticking probability measurements were performed using both the standard King and Wells type reflection technique[18,19] and the previously discussed transient peak-to-peak method.[20] The transient peak-to-peak technique uses a slow-pulsed (2 Hz) beam to accommodate for the fast chamber wall pumping[21] in between each pulse, giving a more reliable base line, whereas the reflection technique uses a fast-pulsed (60 Hz) beam whose base line is strongly affected by chamber wall pumping. The individual resultant signal peaks are used as data points, giving a more accurate initial sticking probability measurement for reactive systems that are sometimes difficult to measure using the standard reflection technique.

B. Computational details

All DFT calculations presented in this paper were performed using the Vienna *ab-initio* simulation package (VASP) (Refs. 22–25) in the generalized gradient approximation (GGA,PW91), with ultrasoft Vanderbilt pseudopotentials[26,27] (as supplied with the VASP program), a 5×4×1 Monkhorst-Pack *k*-point mesh generation scheme (for a total of ten irreducible *k* points), and plane-wave basis kinetic energy cutoff of 350 eV. All parameters (i.e., *k* points, cutoff energy, vacuum space, etc.) were chosen such that they were each individually converged to within 1 meV/atom for the $Cl_{2(g)}/Cl_{(ad)}/Al(111)$ system of study. These calculations should provide good relative accuracy with an estimated relative error 0.1 eV. Regardless of absolute numerical accuracy, the qualitative results from these calculations should be quite reasonable because we are making comparisons both between different bonding geometries and between relative energies, which have all been calculated under identical conditions and with similar types of bonds.

The system studied consisted of an Al(111) surface slab supercell which is repeated in all directions. The aluminum slab was four atomic layers thick, with each layer being 4×5 atoms in area, for a total of 80 Al atoms per unit cell (81 for the adatom calculations). The supercell also contained ten atomic layers of vacuum space (18 Å) in the *z* direction. The bottom two aluminum layers were constrained to the minimum-energy bulk geometry, which was found through a series of bulk Al calculations that yielded an Al nearest-

neighbor distance of 2.86 Å (equal to the experimentally observed value). All other atoms (substrate, adsorbate, gas phase) were allowed to structurally relax without constraint.

III. RESULTS

Experimental identification of the aluminum chloride etch products was not possible with our instrumental setup. The high energy, high fluence photons used during the experiments were too powerful to leave a detectable amount of large-mass fragments behind (but were necessary for a sufficiently measurable Al MPI signal). Therefore, we are left to rely upon both indirect evidence from our own data and the experimental results of several other groups for aid in the identification of the aluminum chloride etch products. All applicable published results for the etching of aluminum by Cl_2 (Refs. 1–9, in particular) were consulted as to their assignment of the major desorption products for this reaction; their reasons for doing so were also taken under consideration. Unfortunately, unlike the results presented in this paper, none of the published studies were performed under ultralow Cl_2 coverage conditions, nor were any of the experiments performed at surface temperatures below $-50\,^{\circ}\mathrm{C}$ ($\sim$220 K). The most similar experimental conditions found in the literature were those presented by Janssen, Kolfschoten, and van Veen[5] who performed molecular beam Cl_2 dosing and TOF-MS detection of thermal etch products from Al(111). The molecular beam flux used for their experiments ($7\times10^{16}\,\mathrm{molecules\,cm^{-2}\,sec^{-1}}$), however, was over three orders of magnitude larger than that used in our experiments.

With this in mind, the major etch products for the etching reaction of Cl_2 on Al(111) reported by van Veen *et al.* are as follows: Al_2Cl_6 at temperatures below 450 K, $AlCl_3$ between 500 and 650 K (also reported by Winters[3]), and AlCl above 700 K. These assignments are generally agreed upon within the bulk of the literature, but with somewhat varying temperature ranges reported across groups. It must also be noted that at the comparatively large pressures under which some of these studies were performed, gas-phase reactions—most importantly the aluminum chloride dimerization reaction, $2AlCl_3 \leftrightarrow Al_2Cl_6$—may play a role in the identity of the final detected etch product. Cleland and Hess[7] showed that at a gas temperature of 500 K, pressures below 1×10^{-5} Torr are required to produce a mean free path long enough that the aluminum chloride desorbates are unlikely to undergo significant intermolecular collisions. Under these conditions, one does not need to account for dimerization because the equilibrium is driven all the way to the left, preventing the formation of Al_2Cl_6. We thus assume that the etch product at 500 K is $AlCl_3$ and at 100 K is either $AlCl_3$ or Al_2Cl_6. This issue will be discussed in more detail later in the paper.

A. Hyperthermal aluminum chloride exit velocities

Time-of-flight spectra of the neutral desorbing aluminum chloride etch products were recorded to determine their exit velocities. This was accomplished by successively increasing the delay between the molecular beam chopper open time and the laser fire trigger by small, successive increments (typically around 2–5 μs per increment). The velocities of the incident Cl_2 molecular beams were measured with a UTI 100C quadrupole mass spectrometer and were checked daily by laser TOF-MS. These checks were performed both to verify that the incident velocities were consistent with the QMS values and to ensure that the arrival times of the incident Cl_2 at the surface were consistent between experiments. Figure 1 presents a typical TOF distribution of each of the incident Cl_2 beams—(a) Cl_2/He, (b) Cl_2/Ne, and (c) pure Cl_2—with the velocities, translational energies, and widths given in the table in part (d). The incident Cl_2 arrival time upon the Al(111) surface t_0 was calculated using both the most-probable velocity of the incident molecular beam $v_{p,inc}$ from the QMS measurements and the measured distance between the laser ionization volume and the aluminum surface $d_{is,inc}$ such that

$$t_0 = \frac{d_{is,inc}}{v_{p,inc}}. \tag{3}$$

This value was then subtracted from the Al^+ TOF spectra in order to provide a zero time for the etch product time-of-flights.

Attempts to fit the time-of-flight data to the commonly used modified Maxwell–Boltzmann distribution form[28,29]

$$f(v) \propto v^3 \exp\left[-\left(\frac{v-v_0}{\alpha}\right)^2\right], \tag{4}$$

where v_0 is the so-called stream velocity and $\alpha = \sqrt{2kT_{\mathrm{eff}}/m}$ is a term describing the width of the distribution via an effective temperature T_{eff} yielded very soft low-correlation fits with large negative stream velocities and large effective temperatures. Such results are not particularly useful, as they only indicate a Boltzmann-type velocity distribution that is wider than a thermal distribution for that particular mean velocity and do not provide any actual numerical information. Therefore, the method described below was used to extract the needed information from the time-of-flight data. Additionally, because the widths of the etch product distributions were found to be 4 to 10 times wider than the incident Cl_2 molecular beam distributions (see Fig. 1), deconvolution of the time-of-flight distributions was not deemed necessary, as the difference between the raw and deconvoluted distributions are negligible.

From the aluminum chloride etch TOF spectra, the most-probable exit velocities [v_p, Eq. (4)] were extracted using the following relationship:

$$v_p = \frac{d_{sl}}{t_p}, \tag{5}$$

where $d_{sl}(=12.5-16.0\,\mathrm{mm})$ is the distance from the surface to the laser focus and t_p is the most-probable time of flight, or the value at the peak detected ion intensity, taken from the TOF spectra. From this data, and with the known etch product masses (Refs. 1–9), the exit kinetic energies can be calculated. These values are then compared to the expected most-probable thermal desorption translational energies E_p for the surface temperatures of interest. E_p is calculated from the expected most-probable time of flights from a general

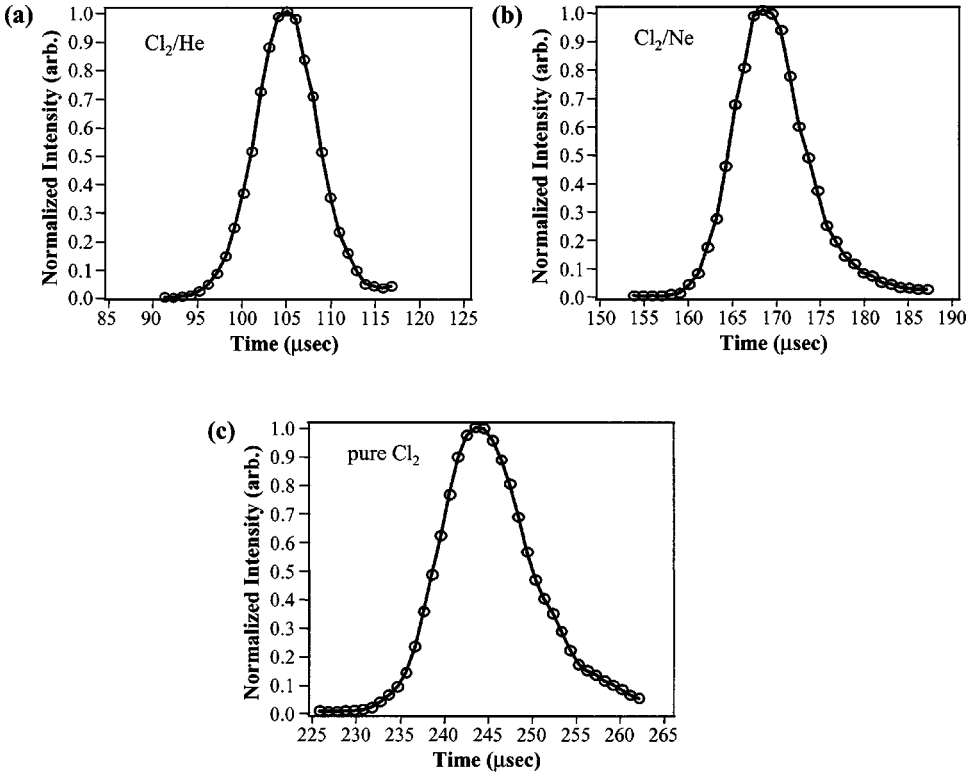

FIG. 1. Time-of-flight distributions for mechanically chopped (7 μs chopper open time) incident molecular beams of (a) 5% Cl_2 seeded in He, (b) 5% Cl_2 seeded in Ne, and (c) pure Cl_2. The table (d) gives the velocities, energies, and widths of the incident Cl_2 beams used in this experiment.

(d)

Species	$v_{p,inc}$ (m/s)	$E_{p,inc}$ (eV)	Width (μs)
Cl_2/He	1327 ± 20.5	0.65 ± 0.02	7.86 ± 0.18
Cl_2/Ne	850 ± 15.9	0.27 ± 0.01	8.66 ± 0.28
pure Cl_2	535 ± 24.9	0.11 ± 0.01	11.13 ± 0.42

flux-weighted Maxwell–Boltzmann time-of-flight distribution using a density detector (as is the case with this detection method),[29]

$$S(t) \propto \frac{1}{t^4} \exp\left(-\frac{m d_{sl}^2}{2kT} \frac{1}{t^2} \right) \Rightarrow \frac{\partial S(t)}{\partial t} = 0 \Rightarrow t_p = \frac{d_{sl}}{2} \sqrt{\frac{m}{kT}}, \tag{6}$$

$$v_p = \frac{d_{sl}}{t_p} = 2\sqrt{\frac{kT}{m}}, \tag{7}$$

$$E_p = \tfrac{1}{2} m v_p^2 = 2kT, \tag{8}$$

where m is the desorption product mass, k is the Boltzmann constant, T is the surface temperature, and t is time of flight; t_p is the most-probable (or peak) time of flight of the distribution, v_p is the most-probable velocity of the distribution, and E_p is the most-probable translational energy of the distribution. In addition, the widths of the measured distributions can be analyzed and compared with the values that would be expected for a thermal distribution. A true flux-weighted Maxwell–Boltzmann thermal distribution of the form given in Eq. (6) exhibits a most-probable velocity to full-width half-max ratio (v_p:w) of about 1, and deviation from this expected ratio is an indication of nonthermal desorption phenomena; a ratio smaller than unity indicates a wider distribution than would be expected for a purely thermal desorption mechanism. All relevant data from the time-of-flight experiments is given in Table I. Two typical raw TOF Al^+ spectra for the 0.27 eV Cl_2 incident beam are shown in Fig. 2, along with thermal distributions for the probable etch products.

1. Low surface temperature desorption

Due to the high sensitivity of the MPI detection scheme, even at low surface temperatures (100 K), very low Cl_2 flux (1.4×10^{13}–4.2×10^{13} molecules cm^{-2} sec^{-1}), and very low surface Cl_2 coverage (<5% monolayer), we are able to observe the small amount of aluminum chloride etch product that results from the gas/surface reaction between Cl_2 and the Al(111) surface. In addition, we find that these etch products desorb from the Al(111) surface with hyperthermal translational exit velocities/energies upon dosing with all incident Cl_2 energies studied. In an effort to consider all reasonable possibilities for etch product identification, as well as to establish both an upper and a lower bound to our measured translational exit energy results at 100 K, we shall compare the kinetic energies of the desorption products assigned as both $AlCl_3$ (lower bound) and Al_2Cl_6 (upper bound).

Figure 3 displays the results of the 100 K Al(111) surface temperature etch product desorption time-of-flight experiments, as both exit velocity vs incident Cl_2 velocity [Fig. 3(a)] and exit translational energy vs incident Cl_2 translational energy [Fig. 3(b)]. The velocity-space graph 3(a) com-

TABLE I. Measured velocities, translational energies, and peak-to-width ratios for desorbing aluminum chlorides at all incident Cl_2 translational energies and Al(111) surface temperatures studied.

Dose species	E_{inc} (eV)	T_s (K)	v_p (m/s)	E_{AlCl_3} (eV)[a]	$E_{Al_2Cl_6}$ (eV)[b]	v_p/w
Cl_2/He: fast[c]	0.65	100	612±21	0.26±0.02	0.52±0.04	0.65±0.06
Cl_2/He: slow[d]	0.65	100	256±9	0.05±0.01	0.09±0.01	0.84±0.08
Cl_2/He	0.65	500	653±16	0.30±0.01	0.59±0.03	0.56±0.02
Cl_2/Ne	0.27	100	518±22	0.19±0.02	0.38±0.03	0.82±0.03
Cl_2/Ne	0.27	500	553±14	0.21±0.01	0.43±0.02	0.76±0.03
pure Cl_2	0.11	100	460±22	0.14±0.01	0.30±0.03	0.69±0.06
pure Cl_2	0.11	500	533±10	0.20±0.01	0.39±0.01	0.71±0.05

[a]Translational energy calculated from mass of $AlCl_3$ etch product and measured v_p.
[b]Translational energy calculated from mass of Al_2Cl_6 etch product and measured v_p.
[c]Fast exit velocity mode; from fresh, clean 100 K surface.
[d]Slow exit velocity mode; from Cl_2 preexposed 100 K surface.

pares the experimentally observed exit velocities with the expected thermal exit velocities for the two possible etch products, $AlCl_3$ and Al_2Cl_6. The energy-space graph 3(b) compares the exit translational energies of the possible etch products (as calculated from the experimental exit velocities) with the expected exit energies from thermal desorption. Exit velocities are also plotted vs both 100 and 500 K Al(111) surface temperatures in Fig. 4.

The desorption products from the reaction at 100 K with the lowest incident translational energy Cl_2 (pure Cl_2, 535 m/s, 0.11 eV) were found to have the slowest monomodal

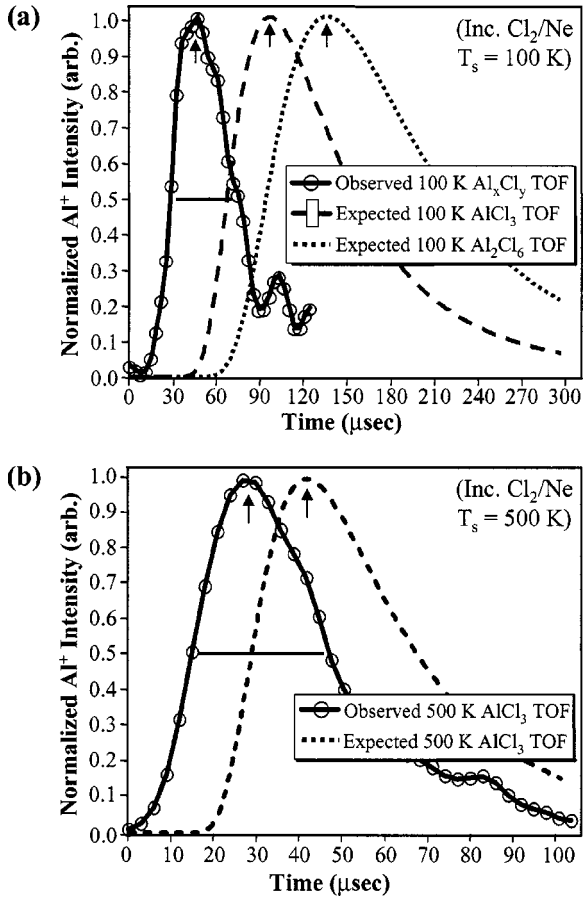

FIG. 2. Maxwell–Boltzmann-type time-of-flight distribution curves for the etch products from the 0.27 eV incident Cl_2 beam on the (a) 100 K and (b) 500 K Al(111) surface. The solid curves show the experimentally observed desorption distribution, and the dashed curves show the expected thermal desorption time-of-flight distributions for the etch product mass and surface temperature of interest, as indicated in the figures. The most probable time-of-flights are indicated by the vertical, single-headed arrows. The full-width half-max of the experimental distributions are indicated by the horizontal, double-headed arrows.

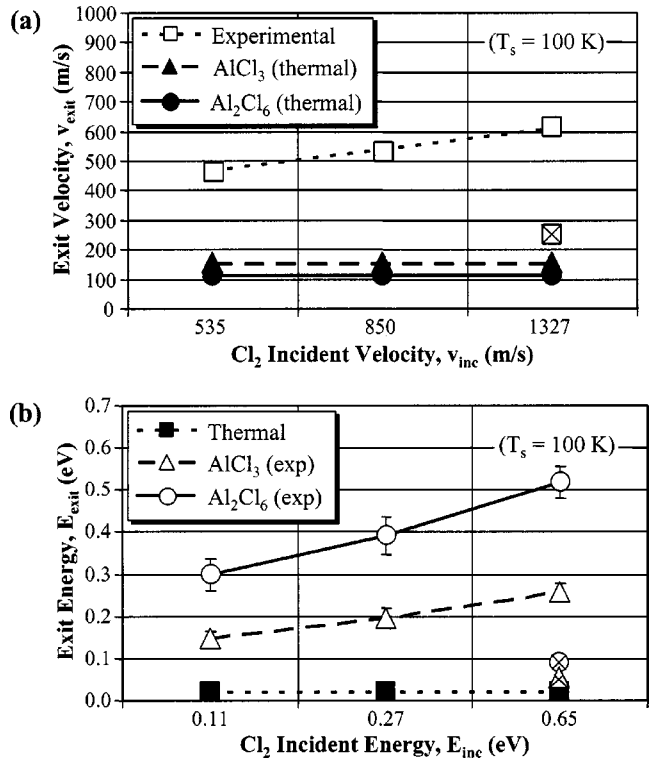

FIG. 3. (a) Etch product exit velocities vs Cl_2 incident velocities for the 100 K Al(111) surface temperature case. The open squares are the experimental velocity data, and the filled circles and triangles represent the expected velocities of the possible etch products from thermal desorption. The anomalous slow component (Cl_2 preexposed surface) is marked with an "*X*." (b) Etch product exit energies vs Cl_2 incident energies for the 100 K Al(111) surface temperature case. The open circles and triangles are the translational energies for the possible etch products as calculated from the experimental velocity data. The filled squares represent the expected translational energy from thermal desorption. The anomalous slow component (Cl_2 preexposed surface) is marked with an *X*. Note: Where experimental error bars are not seen, they are merely obscured from view by the data points.

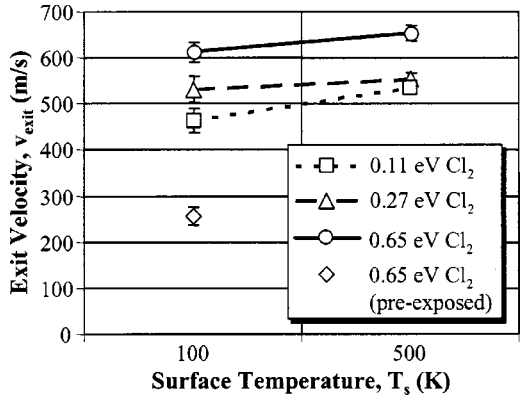

FIG. 4. Experimental aluminum chloride etch product exit velocities vs Al(111) surface temperature. Two exit velocity modes are observed for the 0.65 eV incident energy Cl_2 dose beam at $T_s = 100$ K, where the fast mode results from Cl_2 dosing upon a fresh, clean Al(111) surface and the slow mode results from the Cl_2 preexposed surface. At $T_s = 500$ K with 0.65 eV incident Cl_2 only a monomodal velocity distribution is observed, indicated here with the same shape (open circle, solid line) as the fresh-surface 100 K point.

exit velocity (465 ± 28 m/s). Assuming that the etch product for this system is $AlCl_3$, the measured kinetic energy is 0.14 ± 0.01 eV, or eight times that of 100 K thermal energy (0.017 eV). If we assume that the etch product is Al_2Cl_6, the measured kinetic energy is 0.32 ± 0.04 eV, or 19 times that of the expected thermal exit energy. The 100 K surface temperature 0.11 eV Cl_2 data exhibits a most-probable velocity-to-width ratio ($v_p:w$) of 0.69, consistent with a nonthermal distribution. The etch product mean velocity and the most-probable velocity-to-width ratio ($v_p:w$) for etching by Ne-seeded incident Cl_2 (850 m/s, 0.27 eV) were similar to those from 0.11 eV pure Cl_2.

The etch products from the reaction with the highest incident translational energy Cl_2 (Cl_2/He, 1327 m/s, 0.65 eV) at 100 K were found to be bimodal, with peak velocities of 255 ± 9 m/s and 612 ± 21 m/s. As shown in Fig. 5, during

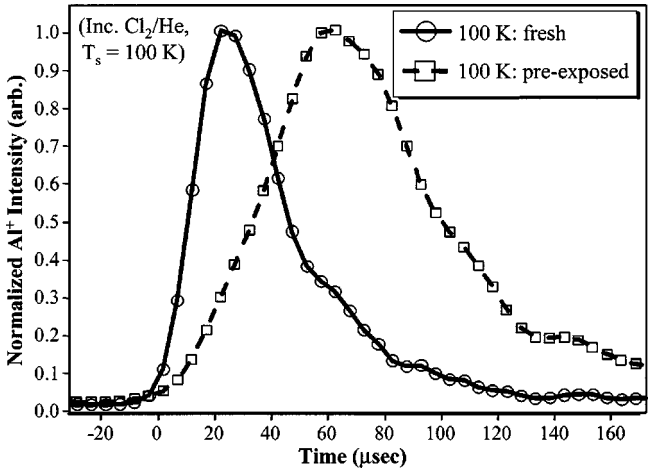

FIG. 5. Two Maxwell–Boltzmann-like time-of-flight distribution curves for the 0.65 eV incident Cl_2 beam and the 100 K Al(111) surface. The solid curve shows the desorption distribution observed upon dosing of a fresh, clean surface, and the dashed curve shows the distribution observed upon dosing of a Cl_2 preexposed surface.

the first ~10 sec of dosing with 0.65 eV Cl_2 on a fresh, clean Al(111) surface, the etch products were found to have the faster exit velocity (solid curve, open circles). After the initial 10 sec clean etch, the peak velocity switches to the lower value (dashed curve, open squares) and remains at this value until surface saturation. Both velocity modes, however, show hyperthermal exit energies. Assuming that the thermal etch product at 100 K is $AlCl_3$, the measured kinetic energy of the slow mode (from the Cl_2 preexposed surface) was 0.05 ± 0.01 eV, three times that of thermal energy, while the fast mode (from the fresh, clean surface) was 0.22 ± 0.03 eV, 13 times that of thermal. Assuming that the etch product is Al_2Cl_6 results in a measured kinetic energy for the slow mode of 0.09 ± 0.01 eV, five times that of thermal, and a fast mode of 0.52 ± 0.04 eV, 31 times greater than thermal energy. The 100 K surface temperature 0.65 eV incident Cl_2 data exhibited a slow-mode $v_p:w$ ratio of 0.65, and a fast-mode ratio of 0.84.

2. High surface temperature desorption

For high surface temperature (500 K), the measured exit velocities/energies of the etch products were not as dramatically larger than thermal as was observed in the cold surface temperature experiments, but were hyperthermal nonetheless (see Fig. 6 and Table I). In this case, all relevant reported experimental data by other research groups identify $AlCl_3$ as the definite etch product at 500 K.[2,3,5,6] As such, we are confident to designate this species as that which we detected in the 500 K experiments. The calculated exit translational energies are shown in Fig. 6(b) and given numerically in Table I.

The most dramatic difference observed at 500 K surface temperature was that the 0.65 eV Cl_2 produced a monomodal etch product velocity distribution instead of the bimodal distribution that was observed at 100 K. At 500 K surface temperature and 0.65 eV incident Cl_2, the measured most-probable velocity was 653 ± 16 m/s. This data exhibits a $v_p:w$ ratio of 0.56, making it the most nonthermal distribution measured. It is possible that the slow etch product observed at 100 K surface temperature and high coverage for 0.65 eV Cl_2 is due to collision induced desorption and is absent at high surface temperature because no adsorbates remain on the surface at 500 K.

Upon comparing the etch product mean velocities at surface temperatures of 100 and 500 K, two major trends are observed. First, as the incident translational velocity is increased by an overall factor of 2.5, the etch product velocity increases by only 22%–33%, with the effect being largest at 100 K surface temperature. Second, as the surface temperature is increased by a factor of 5, the etch product exit velocity increases by only 6.7%–15%, with the effect being largest for the lowest incident energy Cl_2. These trends indicate that there is very little, if any, temperature dependence upon the mechanism of etch product formation and desorption. The weak dependence upon incident Cl_2 velocity/energy is consistent with the existence of two distinct mechanisms for the reaction of Cl_2 with the Al(111) surface—direct activated chemisorption at high incident energy and precursor mediated chemisorption at low incident kinetic

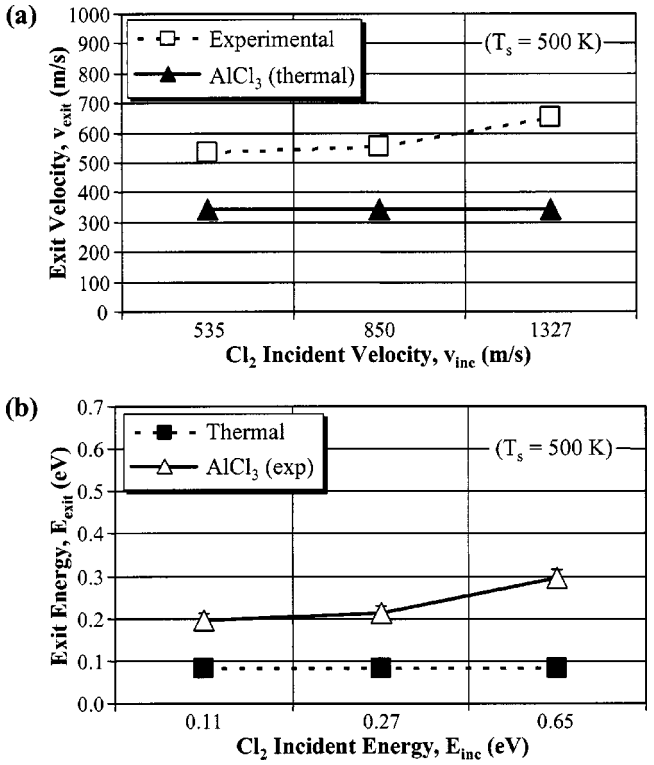

FIG. 6. (a) Etch product exit velocities vs Cl_2 incident velocities for the 500 K Al(111) surface temperature case. The open squares are the experimental velocity data, and the filled diamonds and triangles represent the expected velocities of the possible etch products from thermal desorption. (b) Etch product exit energies vs Cl_2 incident energies for the 500 K Al(111) surface temperature case. The open diamonds and triangles are the translational energies for the possible etch products as calculated from the experimental velocity data. The filled squares represent the expected translational energy from thermal desorption. Note: Where experimental error bars are not seen, they are merely obscured from view by the data points.

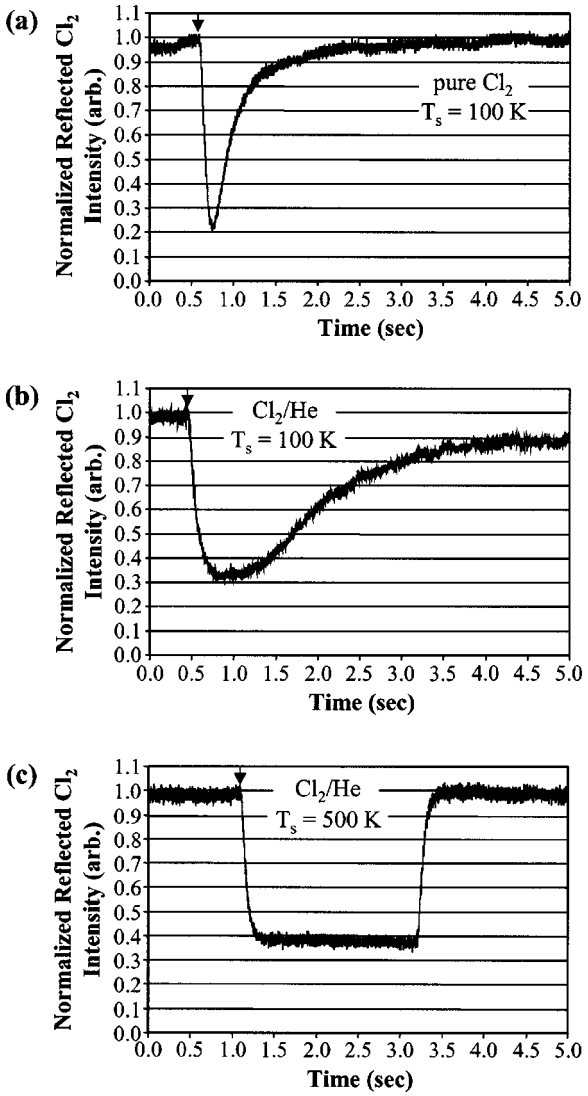

FIG. 7. King and Wells sticking curves for (a) 0.11 eV incident energy Cl_2 on the 100 K surface and 0.65 eV incident energy Cl_2 on both the (b) 100 K surface and the (c) 500 K surface. The beginning of dose beam exposure is indicated on each curve by an arrow.

energy—as described recently.[20] It is reasonable that the different chemisorption mechanisms would produce etch products with slightly different mean velocities. The small amount of excess energy from the direct chemisorption mechanism (high-energy Cl^- adsorbing onto the surface) may add slightly to the overall reaction energetics, consistent with the weak dependence upon Cl_2 incident energy observed for the aluminum chloride exit energies.

B. Cl_2 on Al(111) sticking probabilities

Sticking probability measurements were performed via both the standard King and Wells reflection technique[18,19] and by a transient peak-to-peak method recently discussed by our group.[20] Both techniques used a QMS set for mass 35 as the scattered chlorine detector. The King and Wells and the transient peak-to-peak methods utilize relatively high (60 Hz pulse rate) and low (2 Hz pulse rate) Cl_2 fluxes, respectively, compared to the normal conditions of the time-of-flight experiments. The peak-to-peak method exhibits considerably more sensitivity with respect to initial low-coverage sticking measurements because it can overcome the problems of high flux and chamber wall pumping.[21]

1. Low surface temperature sticking curves

Figure 7(a) displays a typical 100 K Al(111) surface temperature King and Wells type sticking curve for dosing with a 0.11 eV Cl_2 molecular beam, and Fig. 7(b) displays the sticking curve for dosing with a 0.65 eV Cl_2 beam. The 100 K surface temperature sticking curves from both types of sticking experiments demonstrate the basic expected behavior for a reactive system with reasonably high initial sticking probability for all three Cl_2 incident energies (0.11, 0.27, and 0.65 eV). However, the King and Wells technique was found to give artificially low initial sticking probabilities because of the high Cl_2 fluxes and fast pumping by the chamber walls.[21] Upon exposure to the Cl_2 dose beam, a large ($>$65%) initial sticking probability is observed, followed by eventual saturation coverage. The 0.11 eV Cl_2 beam gives the highest initial sticking probability (90%), while the higher-energy 0.27 and 0.65 eV Cl_2 beams show slightly lower (80% and 65%, respectively) initial sticking probabilities. The 0.65 eV Cl_2 sticking curve was found to not reach complete saturation, while the 0.11 and 0.27 eV Cl_2 did

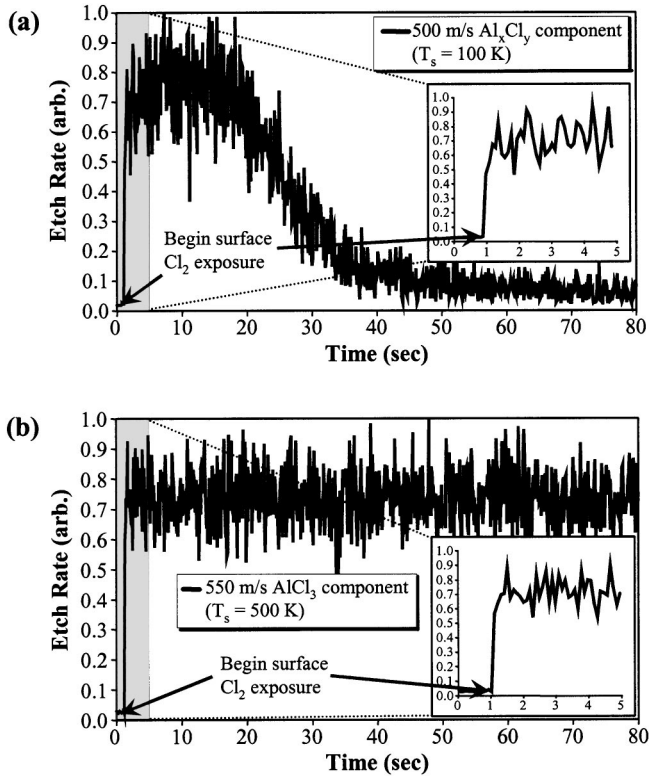

FIG. 8. Etch rate profiles of the 0.27 eV incident energy Cl_2 beam on (a) the 100 K and (b) the 500 K Al(111) surface. The insets are enlargements of the shaded regions and show the first 5 sec of data. Initial Cl_2 exposure is indicated by arrows.

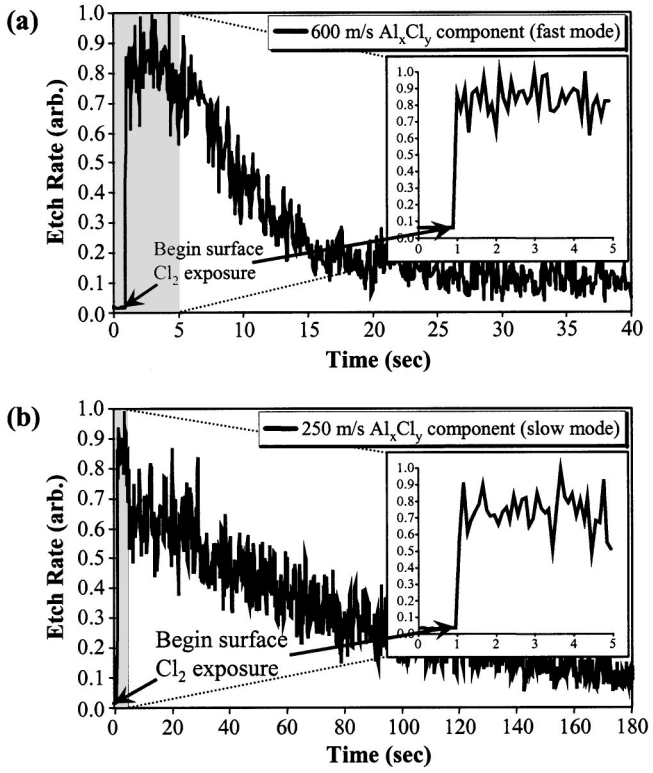

FIG. 9. Etch rate profiles of the 0.65 eV incident energy Cl_2 beam on the 100 K Al(111) surface of (a) the fast mode exit energy Al_xCl_y and (b) the slow mode exit energy Al_xCl_y. The insets are enlargements of the shaded regions and show the first 5 sec of data. Initial Cl_2 exposure is indicated by arrows. Note the change in length of the time axis in (b).

reach complete saturation. Furthermore, the 0.65 eV Cl_2 had a much slower rate of decay toward zero sticking than the 0.11 and 0.27 eV Cl_2.

2. High surface temperature sticking curves

Figure 7(c) displays a typical 500 K Al(111) surface temperature King and Wells type sticking curve for dosing with a 0.65 eV Cl_2 molecular beam. The high surface temperature (500 K) sticking curves from both experiments demonstrate nearly identical behavior for all three Cl_2 incident translational energies. The actual sticking probability values measured are not important, but rather the profile of the curve is critical. At 500 K surface temperature, upon exposure to the Cl_2 molecular beam, steady-state sticking conditions are instantaneously achieved and saturation coverage is never reached. This indicates that an equilibrium is quickly reached between the Cl_2 flux reaching the surface and the etch product desorption.

C. Aluminum chloride etch rate profiles

Fixing the delay between the chopper trigger and the laser fire time (i.e., focusing on one particular exit velocity channel, v_r) allows for the detected ion intensity to be monitored vs elapsed time (see Figs. 8 and 9). In this experiment, the intensity of the detected Al^+ ions is proportional to the rate of desorption of aluminum chloride molecules which exit the surface at a velocity v_r. For these experiments, the most-probable velocity found for each particular system (as presented earlier) was used to select the fixed time-of-flight value t_r such that $v_r = d_{ls}/t_r$. As a check to ensure that the peak positions of the TOF spectra were not actually moving, a number of spectra were taken for the various Cl_2 incident energies and surface temperatures, showing that (aside from the case of 0.65 eV incident Cl_2 at 100 K surface temperature) the observed peak velocity was constant for at least 15 min of dosing. Therefore, we are confident that any changes in the detection intensities found by this experiment are indeed changes in the etch rates, rather than changes in peak exit velocities. The actual etch rates were not calculated in this experiment: the focus of this paper did not warrant such a quantitative study, but rather just a qualitative understanding of the process.

1. Low surface temperature etch rate profiles

The 100 K surface temperature etch rate profiles for the 0.11 and 0.27 eV Cl_2 molecular beam-dosing showed the expected behavior [see Fig. 8(a)] that one would predict from the sticking curves and time-of-flight data. Both incident molecular beam energies yielded detectable etch signal within at most two or three molecular beam pulses. This corresponds to an approximate surface coverage of only about 2%–3% of a monolayer, at which we observe spontaneous etching of the surface. The Al^+ etch curves typically showed a short pseudosteady-state etching region (i.e., a relatively flat etch signal) for the first 20 sec of dosing, followed by an exponential decay to an etch signal of zero. The 0.11 eV incident Cl_2 etch signal decayed to zero with a $1/e$

TABLE II. Final computational relative total energies for DFT-GGA calculations performed on $Cl_{2(g)}/Cl_{(ad)}/Al(111)$ system. The Al(111) slab calculations were performed with the VASP program, using a 5×4×1 Monkhorst–Pack ten *k*-point mesh and plane-wave kinetic energy cutoff of 350 eV.

Geometry	ΔE_{tot} (eV)[a]	Geometry	ΔE_{tot} (eV)[b]
$Cl_{(ad)}$ ontop site	0.00	$3Cl_{(ad)}+Al_{(ad)}$	0.00
$Cl_{(ad)}$ bridge site	0.16	$AlCl_{3,(ad)}$ (Al hollow, Cl hollow)	−0.67
$Cl_{(ad)}$ hollow site	0.29	$AlCl_{3,(ad)}$ (Al hollow, Cl ontop)	−0.70
Clustered[c] $Cl_{(ad)}$; bridge sites[d]	0.11	$AlCl_{3,(ad)}$ (Al ontop, Cl bridge)	−0.70
Clustered $Cl_{(ad)}$; ontop sites	0.18	$AlCl_{3,(g)}$: desorbed	−0.05

[a]Difference in DFT total energies (per Cl adsorbate), with respect to the "$Cl_{(ad)}$ hollow-site" total energy.
[b]Difference in DFT total energies, with respect to the non-bonded "$3Cl_{(ad)}+Al_{(ad)}$" total energy.
[c]Initial clustered geometry, with Cl adsorbates in adjacent hollow sites.
[d]Final relaxed geometry; Cl adsorbates moved from adjacent hollow-sites to nearby bridge-sites during relaxation.

lifetime of 10 sec, and the 0.27 eV incident Cl_2 system showed a 1/*e* lifetime of about 8 sec. The variation in lifetimes most likely stems from a combination of slightly differing Cl_2 fluxes at the surface, small differences in sticking probabilities, and slight dissimilarities in the actual etch rates for the two different energy incident beams. These times are also longer than those in the sticking experiments due to the difference in Cl_2 molecular beam flux (60 Hz unchopped beam for the King and Wells sticking experiments vs 10 Hz chopped beam for the etch rate profiles and time-of-flight experiments).

Two different modes of etch behavior are observed for 100 K surface with the 0.65 eV incident Cl_2 beam, as shown in Fig. 9. Figure 9(a) displays an etch rate profile curve for 100 K surface temperature Al(111) exposed to a 0.65 eV Cl_2 beam while monitoring the fast velocity mode (600 m/s), and Fig. 9(b) displays the profile curve for the same system while monitoring the slow velocity mode (250 m/s). The first, and fastest, etch mode is found for very low surface coverages (total dosing time of=10 sec), exhibiting a pseudosteady-state region lasting for the first 5–6 sec of dosing and a subsequent decay lifetime of about 4 sec. This behavior corresponds to the fast mode seen in the TOF experiments. The second, slower mode is found at slightly higher surface coverages (total dosing time of>10 sec) or from Cl_2 preexposed surfaces. In this mode, the pseudosteady-state region lasts longer (~15 sec) and has a longer decay lifetime (~60 sec). Both velocity modes exhibit the same instantaneous etch product signal within ~1% monolayer (ML), surface coverage as was seen with the 0.11 and 0.27 eV incident Cl_2 energy beams.

2. High surface temperature etch rate profiles

Figure 8(b) shows an etch rate profile for 500 K surface temperature Al(111) exposed to a 0.27 eV incident translational energy Cl_2 beam. The high surface temperature etch rate profiles recorded in this experiment all exhibit the same basic behavior, independent of incident Cl_2 kinetic energy. As with the 100 K surface temperature studies, all three incident molecular beam energies yielded a detectable steady-state etch signal within, at most, two or three molecular beam pulses. This corresponds to an approximate surface coverage of only about 2%–3% ML, which is the minimum coverage at which we observe spontaneous etching of the surface. The etch rate profiles for the elevated surface temperatures also displayed instantaneous steady-state conditions that lasted for the entire span of the experimental run time (at least 15 min of continual dosing). Therefore, not only does the surface immediately begin to etch upon exposure to small amounts of Cl_2 (<5% monolayer), but it continues to etch indefinitely at exactly the same rate.

D. Computational data

DFT calculations under periodic boundary conditions, with Vanderbilt-type ultrasoft pseudopotentials and plane-wave basis were performed on the $Cl_{2(g)}/Cl_{(ad)}/Al(111)$ system in an effort to provide information concerning both the possible surface reactions and the energetics of those reactions. The goal was to study the nature of the adsorption of Cl on the Al(111) surface, including adsorption site preference and possible Cl adsorbate clustering effects on flat terraces. Calculations were also performed to help characterize the model reaction sequence occurring in the present study,

$$\tfrac{3}{2}Cl_{2,(g)} \xrightarrow{Al(111)} 3Cl_{(ad)}+Al_{(ad)} \xrightarrow{Al(111)} AlCl_{3,(ad)} \xrightarrow{Al(111)} AlCl_{3,(g)}. \quad (9)$$

Namely, this total reaction includes the dissociation of incident Cl_2 and adsorption of Cl fragments products onto the Al(111) surface, the reaction of Cl adsorbates with an Al adatom to form ground state $AlCl_3$ (as standard DFT only allows for the calculation of ground state energies and properties), and the desorption of ground state $AlCl_3$ from the Al(111) surface. Note that the above reaction equation does not explicitly state by which chemisorption mechanism the Cl adsorbates are produced; it states only that a total of three Cl atoms are required and the overall products can result from any combination of Cl_2 molecules (two or three) and chemisorption mechanisms (direct abstractive or precursor mediated). The computational results concerning relative total energies for these calculations can be found in Table II, and those directly associated with the above reaction sequence are presented diagrammatically in Fig. 10(a).

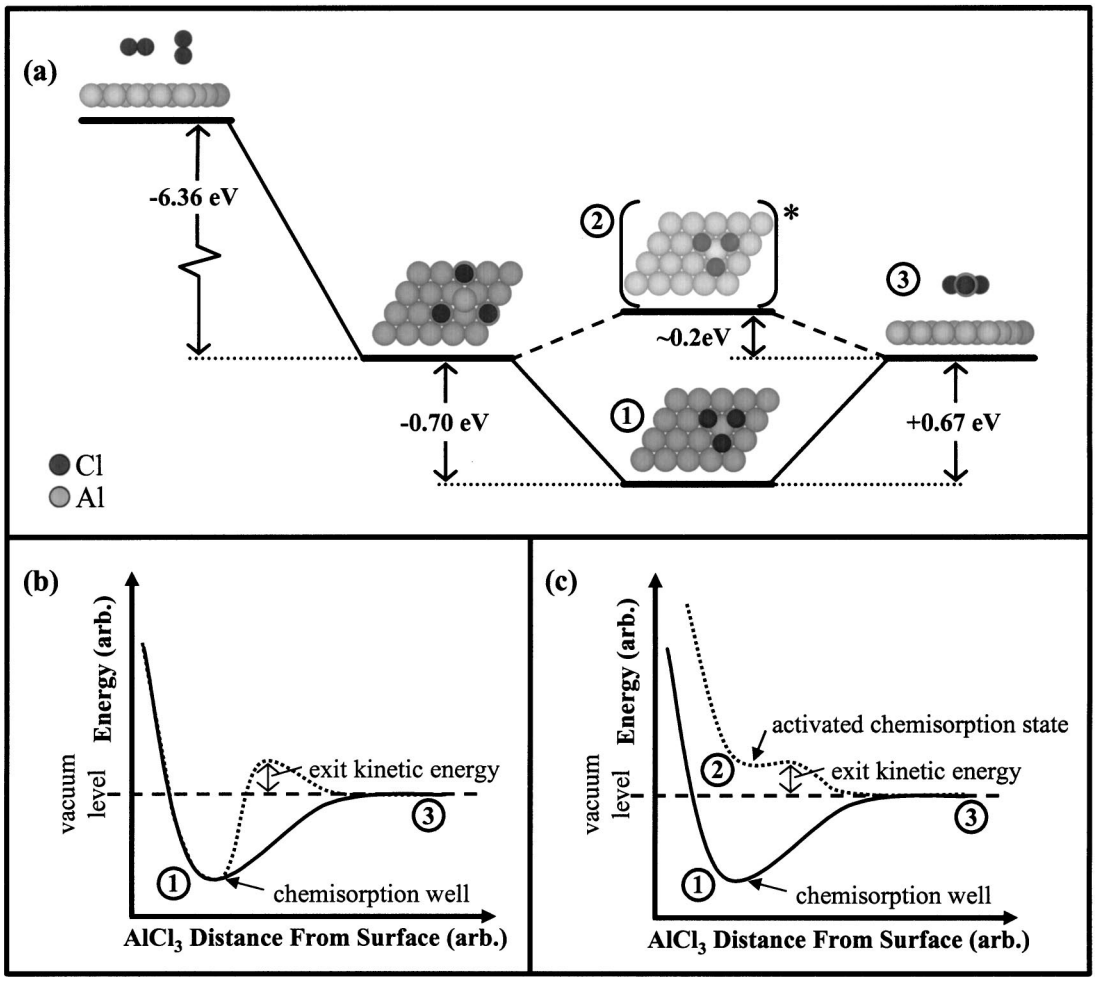

FIG. 10. Computational (DFT) energy diagram (a) of the Cl_2 dissociation/adsorption reaction, followed by subsequent $AlCl_3$ etching from both the ground-state chemisorbed and the activated chemisorbed $AlCl_3$ (labeled 1 and 2, respectively). Conceptual potential diagrams for $AlCl_3$ chemisorption/desorption are given for the (b) activated desorption and the (c) activated chemisorption state models for hyperthermal exit velocity of aluminum chloride etch products from low-coverage Cl_2 on Al(111). Points of interest between the reaction energy diagram and the corresponding position on the potential diagrams are signified by the circled numbers. The data presented in this paper is consistent with the activated chemisorption state model (c) rather than the activated desorption model (b).

1. Cl Adsorption on Al(111)

The first reaction of interest in this sequence is the dissociation of gas phase Cl_2 and the subsequent adsorption of the resultant Cl atoms onto the Al(111) surface: $\frac{3}{2}Cl_{2,(g)} \xrightarrow{Al(111)} 3Cl_{(ad)}$. As discussed previously,[20] the dissociation/adsorption reaction of Cl_2 on Al(111) proceeds via two different pathways: direct abstractive chemisorption (remote dissociation) and indirect precursor-mediated chemisorption (surface dissociation). In the direct mechanism, as a Cl_2 molecule approaches the Al(111) surface an electron can be transferred from the Fermi sea of the metal to the Cl_2, instantly creating a Cl_2^- molecular ion. This ion resides high on the repulsive part of the intermolecular potential, resulting in dissociation into a Cl^- ion and a neutral Cl fragment. Note that the closer the Cl_2 is to the surface at the moment of the electron transfer, the higher on the repulsive part of potential the ion will reside. The final result is that the Cl^- ion is drawn to the surface and eventually chemisorbs while the neutral Cl is ejected back into the gas phase. In contrast, for the indirect mechanism, dissociation occurs after the neutral molecule has reached the surface (without being ionized) and has been subsequently trapped in a shallow physisorption state. Dissociation in this manner, while dependent upon the Cl_2 incident molecular orientation with respect to the surface, can either result in the ejection of a Cl neutral into the gas phase and a single Cl adsorbate, or it can result in the adsorption of both Cl atomic fragments. However, regardless of the mechanism, the final chemisorption energies (bond strengths) for Cl onto Al(111) will be the same.

The energetics for the Cl_2 dissociation/adsorption reaction on Al(111) were calculated using the total energy difference between a system consisting of two Cl noninteracting adsorbates on the Al(111) surface and a system consisting of a Cl_2 molecule residing in the gas phase above the Al(111) surface. The calculated reaction energy per Cl adsorbate was -2.12 eV with respect to molecular chlorine far from the surface; for the given reaction, $\frac{3}{2}Cl_{2,(g)} \xrightarrow{Al(111)} 3Cl_{(ad)}$, the total reaction energy is -6.36 eV. The various dissociation/adsorption mechanisms were considered, and calculations were performed to check for consistency in the final overall

reaction energy with respect to mechanism and method.

In searching for the lowest-energy (i.e., most stable) adsorption sites for the Cl adsorbates, it was found that adsorbates strongly prefer ontop sites over both bridge and threefold hollow sites. The relaxed geometries of the Cl adsorbate calculations also show that the Cl atoms tend to pull the Al atoms to which they were bonded into positions that are above the average terrace plane. In addition, the Al atoms that occupied the nearest-neighbor positions were found to have physically relaxed into the resulting voids, placing them in positions that are slightly below the average terrace plane. Overall, the largest displacement in the *z* direction was observed for the final $Cl_{(ad)}$ ontop site geometry, where the bonded Al atom was pulled to a position of over 0.4 Å above the terrace plane. The displacements seen in the final hollow site and bridge site geometries were similar to those of the ontop site geometry, but smaller in magnitude by at least a factor of 2.

The low-temperature ion-assisted etch model forwarded by Ikawa *et al.*[9] included the formation of two-dimensional clusters of Cl adsorbates on the Al(111) surface to help explain the enhancement of the low-temperature etch rate in an ECR plasma. To test this hypothesis, adsorbate clusters containing three $Cl_{(ad)}$ atoms residing in nearest-neighbor equivalent sites (i.e., ontop-ontop-ontop, bridge-bridge-bridge, and hollow-hollow-hollow clusters, all in a triangular geometry) were allowed to structurally relax. It was found that each of these clusters were unstable, and that repulsions between the $Cl_{(ad)}$ atoms forced them to physically move away from each other on the surface, giving final interatomic distances of at least 4 Å. Even after the minimization of interatomic forces, the total energy of the initially-ontop-clustered $Cl_{(ad)}$ system (the system with the lowest relative total energy) was found to be higher than that of the dispersed ontop $Cl_{(ad)}$ system by 0.3 eV. As a result, we believe that clustering of Cl adsorbates, even at temperatures as low as 100 K, is unlikely.

2. Formation and desorption of $AlCl_3$

The reaction involving the formation of adsorbed $AlCl_3$, $3Cl_{(ad)} + Al_{(ad)} \xrightarrow{Al(111)} AlCl_{3,(ad)}$, was modeled computationally using an aluminum adatom and three nearby chlorine adsorbates. The Al adatom, rather than a standard surface atom, was chosen for use as the reaction center in an effort to model Al atom defect sites such as step-edges and regrowth islands (as well as actual adatoms). These unique sites are more exposed to surface adsorbates in the low-coverage regime and provide a good model system for this set of conditions. The formation energy was calculated by subtracting the total energy of the nonbonded reactant system from the total energy of the $AlCl_3$ adsorbate system: $\Delta E_f = E_{\text{tot}}(AlCl_3) - E_{\text{tot}}(Al+3Cl)$. Note that for the nonbonded reactant system, the Cl adsorbates were positioned outside of the bonding range of the Al adatom, and after structural relaxation yielded no attractive forces toward the Al adatom. To ensure that both the products and the reactants were all in the lowest energy geometric configurations possible, multiple adsorption geometries were considered. The Al adatoms energetically preferred hollow site positions, while the Cl adsorbates remained most stable in their preferred ontop site positions. The $AlCl_3$ adsorbates showed no adsorption geometry preference within the estimated accuracy of the calculations (i.e., the $AlCl_3$ surface adsorption potential was essentially noncorrugated). The final value calculated from these simulations showed an $AlCl_{3,(ad)}$ formation energy of -0.70 eV with respect to the separate $Al_{(ad)}$ atom and $3Cl_{(ad)}$ atoms on the Al(111) surface.

The final step of this reaction sequence is the desorption of the ground state $AlCl_3$ adsorbate into the gas phase, $AlCl_{3,(ad)} \xrightarrow{Al(111)} AlCl_{3,(g)}$. We can only consider ground state energies, as standard DFT is unable to predict excited states. The final desorption energy, $\Delta E_f = E_{\text{tot}}(AlCl_{3,(g)}) - E_{\text{tot}}(AlCl_{3,(ad)})$, was calculated to be $+0.67$ eV. The positive value indicates that the desorption of the ground state etch product is endothermic in this case. In other words, the bottom of the chemisorption well for ground state $AlCl_3$ on the Al(111) surface is 0.67 eV below the vacuum level. This means that if the ground state $AlCl_3$ is to exit the surface with a translational energy of 0.2 eV, it must overcome first the 0.67 eV deep potential well and then a barrier to desorption of about 0.2 eV, for a total energy requirement of about 0.87 eV. We would like to restate that these calculated energies describe the ground state system only and do not account for any excited state properties or energies. We will show, however, that the existence of such excited states can indeed account for the hyperthermal desorption of $AlCl_3$.

E. Etch product identification

We now return to the task of etch product species assignment. Our previous assumptions, based upon reports in the literature by Winters[3] and Janssen, Kolfschoten, and van Veen,[5] lead to the conclusion that the major etch product detected in the 500 K surface temperature experiments was $AlCl_3$. Recall that $AlCl_3$ was reported by Janssen *et al.* as the major etch species at pressures around 7.5×10^{-7} Torr (Cl_2 surface flux of 7×10^{16} molecules cm^{-2} sec^{-1}) and temperatures between 450 and 750 K. Our experiments have made use of a much lower flux (1.0×10^{13}–3.0×10^{13} molecules cm^{-2} sec^{-1}), and therefore lower pressure molecular beam (i.e., no postdesorption dimerization), and we have shown that the etch products are hyperthermal regardless of which species of aluminum chloride we utilize for data analysis. We can also eliminate AlCl as a possible etch product at 500 K due to its high binding energy to the substrate.[5] After these considerations are taken into account, we state with confidence that $AlCl_3$ is the etch product at 500 K surface temperature.

The etch product identity at 100 K surface temperature is, however, a matter of some question. All previous experiments performed near room temperature report an Al_2Cl_6 etch product, but these were carried out under considerably higher Cl_2 fluxes ($>7\times10^{16}$ molecules cm^{-2} sec^{-1}), surface coverages (>1 ML), and pressures ($>7.5\times10^{-7}$ Torr) than were our experiments. One must note that it is under these conditions that postdesorption chemistry may occur. Consideration of the very low Cl_2 incident fluxes (1.0×10^{13}–3.0×10^{13} molecules cm^{-2} sec^{-1}) and surface coverages (1%–3% ML) at which spontaneous etching was

observed in our experiments leads us to believe that postdesorption gas-phase dimerization reactions were nonexistent and that any aluminum chloride etch products were detected as desorbed, as either $AlCl_3$ or Al_2Cl_6. The very low surface coverages also make reasonable the assumption that the concentration of Cl adsorbates on the Al(111) surface at the onset of spontaneous etching was too small to provide for the formation of a large amount of surface Al_2Cl_6 species, especially since the etching begins with the equivalent of 1% ML Cl_2 surface dose, as shown in the etch rate profiling experiments. Finally, we note that the exit velocities of the etch products at both the 100 and 500 K surface temperatures were essentially equal (with the exception of the anomalous slow mode at 100 K surface temperature and 0.65 eV incident Cl_2), strongly indicating that the identity of the etch products at both temperatures are indeed identical. Therefore we assert with confidence that the etch product specie at 100 K in our ultralow coverage experiments is $AlCl_3$. It is possible, however, that the etch product being detected in the anomalous slow, high-coverage mode may very well be Al_2Cl_6.

IV. DISCUSSION

A. Fast chlorine adsorbate agglomeration

A high rate of reaction of the adsorbed $Cl_{(ad)}$ on the Al(111) surface to form $AlCl_{3(ad)}$ is consistent with the significant etch product desorption observed at the very low coverage (<5% monolayer) conditions under which the time-of-flight experiments were performed. Indeed, Park *et al.* forwarded a model consisting of fast surface diffusion and agglomeration of Cl adsorbates, and fast subsequent reaction rates of intermediates on the Al surface, as ion bombardment was found to have no effect on the etch rate.[4] Our experimental sticking probability results are also consistent with a fast diffusion/agglomeration mechanism, and the aluminum chloride etch rate profiles provide directly observable evidence of unusually fast etch product formation in this system.

The etch rate profiles show aluminum chloride desorption products within just two or three molecular beam pulses, which corresponds to a surface coverage of less than 5% of a monolayer. Such a phenomenon is only possible if there exists a mechanism of fast agglomeration of the Cl adsorbates into reactive positions on the aluminum surface that creates the observable $AlCl_3$ gas-phase etch products. The data is consistent with the fast diffusion of the Cl adsorbates across the Al(111) surface, such that molecules, or even small islands, of aluminum chlorides are produced and then immediately desorb.

DFT-GGA slab calculations performed on a model $Cl_{(ad)}$/Al(111) system indicate that there is a reasonable thermodynamic drive toward adsorbate agglomeration around and reaction with Al adatoms: the formation of the $AlCl_3$ etch products is exothermic by 0.70 eV per molecule. It is likely that this favorable reactivity would also be seen at Al regrowth islands and step edges. Sufficient numbers of such sites should exist on the surface to account for the significant initial etch rates seen in our low-coverage experiments. The 100 K sticking probability and etch rate measurements are also consistent with the hypothesis that etching occurs favorably at adatoms, regrowth islands, and step edges. At low temperatures, etching is quickly quenched and the surface becomes saturated with Cl adsorbates because there is insufficient thermal energy to regenerate the reactive sites. In contrast, we observe in the 500 K sticking probability and etch rate measurements that surface saturation is never reached and that etching is never quenched, indicating that enough thermal energy exists to regenerate the highly reactive etch sites under these conditions. It should be noted that a defect-dependent mechanism such as the one we propose here is likely to exhibit effects related to the surface history. Effects of this nature may be observable in the low temperature sticking or etch rate experiments, where a slight increase in the length of the initial etching rate is expected and yields a longer time to surface saturation. We did not pursue in depth experiments concerning this issue, though, because these effects would best be probed with low-temperature scanning tunneling microscopy, whereby one could quantitatively account for the number and type of defect sites on the surface; such experiments are beyond the scope of the present study.

Our calculations also indicate that adsorbed Cl atoms tend to pull the adjacent Al surface atoms out of the surface plane by as much as 0.4 Å. The fact that the second-nearest neighbor Al atoms then sink into the partial voids left behind provides for an even larger relative atomic displacement for the affected Al surface atoms. It is possible that displaced surface atoms such as these would be more prone to both attack and removal by nearby Cl adsorbates (similar to the Al adatom case). It is also possible that this displacement could reduce the energy requirements for Al adatom/vacancy creation. However, such an effect was not directly observed in the calculations because only single-point and geometry relaxation DFT calculations, which are carried out at a computational temperature of 0 K, were performed, not actual molecular dynamics simulations.

B. Activated chemisorption states

Hyperthermal etch product exit velocities, such as those observed in our low-coverage Cl_2/Al(111) system experiments, can be explained with four possible mechanistic models: first, activated desorption, in which the ground state aluminum chloride chemisorption potential well lies below the vacuum level and a barrier to desorption resides above the vacuum level [see Fig. 10(b)]; second, activated chemisorption states, in which there exists at least one aluminum chloride adsorption state with a potential well at an energy above the vacuum level [see Fig. 10(c)]; a third case in which the energy of reaction is channeled into translational energy for the desorbing aluminum chloride; and finally, collision-induced desorption.

The latter two models can be easily eliminated from consideration. It is unlikely that any reasonable amount of excess energy from the formation of aluminum chlorides could be sufficiently channeled into translational energy, as it is well known that localized energy dissipates quickly on metal surfaces. Dynamics simulations concerning the dissociative

chemisorption of O_2 on Al(111) have found that the transfer of energy to the substrate lattice is much too effective to allow for a large post-dissociation adsorbate mobility.[30–32] For the O_2/Al(111) system, there is a much higher exothermicity than for the Cl_2/Al(111) reaction (-7.95 eV per site with respect to the free oxygen atom), indicating that this mechanism is unlikely and can be eliminated. It is also unlikely that collision-induced desorption could produce etch products with such high translational energies, especially at low surface coverages (<5% monolayer). It is possible that at high surface temperatures (500 K) and high incident kinetic energy there may be components of the etch product translational energy that are produced via collision-induced desorption; this would slightly increase the measured most-probable etch product exit velocity for the high-energy (0.65 eV) incident Cl_2 beam. However, this mechanism is not expected to play a role for the lower energy incident Cl_2 beams (0.11 and 0.27 eV) or on the low temperature (100 K) surface.

It is necessary at this point to distinguish between the activated desorption and the activated chemisorption state models for our system of study. Our basic calculations cannot be used to directly predict a desorption mechanism in this case because DFT is known to be inaccurate in predicting barrier heights and weak binding potentials. We can, however, use the calculated desorption energy values to support our mechanistic assertions. Because we observe hyperthermal exit velocities at 100 K, the activated desorption model seems inconsistent with the data, as it is unlikely that the etch products could easily surmount such an activation barrier at this temperature. According to the DFT calculations and the measured exit translational energies, the barrier height for ground state $AlCl_3$ desorption would be a total of about 0.87 eV, which is considerably large at these temperatures (100–500 K). Therefore, we assert that our results are most consistent with the existence of aluminum chloride activated chemisorption states on the Al(111) surface, desorption from which results in hyperthermal etch product velocities.

V. CONCLUSIONS

Hyperthermal desorption of aluminum chloride etch products from Cl_2/Al(111) has, for the first time, been observed under low coverage conditions (<5% monolayer) at both low (100 K) and high (500 K) surface temperatures and at a variety of incident Cl_2 kinetic energies. Etching is found to spontaneously begin immediately upon exposure of the Al(111) surface to pulsed molecular beams of Cl_2. We believe these hyperthermal desorption products are only observable under very low Cl_2 fluxes and/or surface coverages, and have thus not previously been seen in high coverage experiments. The model presented here to explain these phenomena includes a combination of both fast Cl adsorbate diffusion and agglomeration at Al step-edges, regrowth islands, and adatoms, with fast formation of $AlCl_3$, and the existence of activated aluminum chloride chemisorption states with potential energies above the vacuum level.

ACKNOWLEDGMENTS

The authors would like to thank D. Auerbach of Hitachi Global Storage Technologies for valuable discussions and insights into the analysis of our time-of-flight data, and D. Sorescu of the University of Pittsburgh for discussions concerning the aluminum slab DFT computational work. This work was supported by the National Science Foundation, Grant No. NSF-CHE0074813.

[1] D. L. Smith and P. G. Saviano, J. Vac. Sci. Technol. **21**, 768 (1982).
[2] D. L. Smith and R. H. Bruce, J. Electrochem. Soc. **129**, 2045 (1982).
[3] H. F. Winters, J. Vac. Sci. Technol. B **3**, 9 (1985).
[4] S. Park, L. C. Rathburn, and T. N. Rhodin, J. Vac. Sci. Technol. A **3**, 791 (1985).
[5] R. J. A. A. Janssen, A. W. Kolfschoten, and G. N. A. van Veen, Appl. Phys. Lett. **52**, 98 (1988).
[6] D. A. Danner and D. W. Hess, J. Appl. Phys. **59**, 940 (1986).
[7] T. A. Cleland and D. W. Hess, J. Vac. Sci. Technol. B **7**, 35 (1989).
[8] N. N. Efremow, M. W. Geis, R. W. Mountain, G. A. Lincoln, J. N. Randall, and N. P. Economou, J. Vac. Sci. Technol. B **4**, 337 (1986).
[9] T. Uchida, H. Aoki, M. Hane, S. Hasegawa, and E. Ikawa, Jpn. J. Appl. Phys., Part 1 **32**, 6095 (1993).
[10] J. W. Lutze, A. H. Perera, and J. P. Krusius, J. Electrochem. Soc. **137**, 249 (1990).
[11] T. Smith, Surf. Sci. **32**, 527 (1972).
[12] V. M. Bermudez and A. S. Glass, J. Vac. Sci. Technol. A **7**, 1961 (1989).
[13] J. Bormet, J. Neugebauer, and M. Scheffler, Phys. Rev. B **49**, 17242 (1994).
[14] T. F. Hanisco, C. Yan, and A. C. Kummel, J. Chem. Phys. **95**, 6178 (1991).
[15] T. F. Hanisco and A. C. Kummel, J. Phys. Chem. **95**, 8565 (1991).
[16] K. A. Pettus, T. S. Ahmadi, E. J. Lanzendorf, and A. C. Kummel, J. Chem. Phys. **110**, 4641 (1999).
[17] K. A. Pettus, P. R. Taylor, and A. C. Kummel, Faraday Discuss. **117**, 321 (2000).
[18] D. A. King and M. G. Wells, Surf. Sci. **29**, 454 (1972).
[19] D. A. King and M. G. Wells, Proc. R. Soc. London, Ser. A **339**, 245 (1974).
[20] G. C. Poon, T. J. Grassman, J. C. Gumy, and A. C. Kummel, J. Chem. Phys. **119**, 9818 (2003).
[21] B. Berenbak, D. A. Butler, B. Riedmuller, D. C. Papageorgopoulos, S. Stolte, and A. W. Kleyn, Surf. Sci. **414**, 271 (1998).
[22] G. Kresse and J. Hafner, Phys. Rev. B **47**, 558 (1993).
[23] G. Kresse, thesis, Technische Universität Wien, 1993.
[24] G. Kresse and J. Furthmüller, Comput. Mater. Sci. **6**, 15 (1996).
[25] G. Kresse and J. Furthmüller, Phys. Rev. B **54**, 11169 (1996).
[26] D. Vanderbilt, Phys. Rev. B **41**, 7892 (1990).
[27] G. Kresse and J. Hafner, J. Phys.: Condens. Matter **6**, 8245 (1994).
[28] D. J. Auerbach, in *Atomic and Molecular Beam Methods*, edited by G. Scoles (Oxford University Press, New York, 1988), Vol. 1, Chap. 14, pp. 362–379.
[29] F. M. Zimmermann and W. Ho, Surf. Sci. Rep. **22**, 127 (1995).
[30] C. Engdahl and G. Wahnström, Surf. Sci. **312**, 429 (1994).
[31] J. Jacobsen, B. Hammer, K. W. Jacobsen, and J. K. Nørskov, Phys. Rev. B **52**, 14954 (1995).
[32] G. Wahnström, A. B. Lee, and J. Strömquist, J. Chem. Phys. **105**, 326 (1996).